Article

Induction generator with direct control and a limited number of measurements on the side of the converter connected to the power grid

Andrzej Kasprowicz [1,*] , Ryszard Strzelecki [2,*]

[1] Faculty of Electrical Engineering, Gdynia Maritime University, 81-225 Gdynia, Poland;
[2] Faculty of Electrical and Control Engineering, Gdańsk University of Technology, 80-233 Gdańsk, Poland;
[*] Correspondence: a.kasprowiczcz@we.umg.edu.pl (A.K.); ryszard.strzelecki@pg.edu.pl (R.S.)

Abstract: The article presents an induction generator connected to the power grid using the AC / DC / AC converter and LCL coupling filter. In the converter, both from the generator side and from the power grid side, three-level inverters were used. The algorithm realizing Pulse Width Modulation (PWM) in inverters has been simplified to the maximum. Control of the induction generator was based on the Direct Field Oriented Control (DFOC) method. At the same time, voltage control has been used for this solution. The MPPT algorithm has been extended to include the variable pitch range of the wind turbine blades. The active voltage balancing circuit has been used in the inverter DC voltage circuit. In the control system of the grid converter with an LCL filter, the number of measurements was limited to the measurement of power grid currents and voltages. Synchronization of control from the power grid side is ensured by the use of a PLL loop with the system of preliminary suppression of undesired harmonics (CDSC).

Keywords: induction generator; Direct Field Oriented Control (DFOC), three-level inverter; sinusoidal pulse width modulator (SPWM), maximum power point tracking (MPPT)

1. Introduction

Small wind power plants are becoming more and more popular as sources of electric energy. They are mainly based on asynchronous machines. It is a cheaper solution compared to the use of synchronous generators with electromagnetic excitation or permanent magnets. The machine itself is also much simpler and therefore more reliable. It can also be directly connected to the power grid in generator mode. Such a direct connection to the power grid does not require a special synchronization mode, which is a very important issue. However, it is only possible to produce and deliver electricity to the grid above a certain wind speed. There is also no possibility of electric control of active power output. When the machine is directly connected to the power grid, there is a demand for reactive power. This degrades the energy quality near the installation of such a generator. Accordingly, in order to improve the quality of the energy, there is a need for reactive power compensation. In the simplest solution, it is a bank of capacitors. In more advanced systems, power electronics systems are used.

The above drawbacks of direct connection of the generator to the power grid in the context of current requirements related to combining new energy sources have considerably limited the possibilities of its application in recent times.

Currently, in order to eliminate the negative impact of the new energy sources connected to the power grid, various types of power electronic converters are used. They implement connections of newly connected sources to the power grid without introducing distorted currents to it. Currents similar to sinusoidal are obtained by means of the control and application of the LCL filter. The use of power converters from the generator

side and the power grid side has led to full conversion of the generated energy [1,2,3,4,5]. It also created the possibility of controlling the active power given to the power grid.

An additional functionality of using converters is also the ability to control the reactive power. This solution also extends the wind speed range for which the power plant is able to transmit energy to the grid. The extension of the scope applies to both lower and higher wind speeds at which currently existing systems have to already be disconnected.

Also, thanks to the fact that the system has full conversion of electrical energy, it was possible to implement the tracking of the maximum power generated by the generator in a wide range of wind speed.

There are many methods to track the maximum power [4,6-12]. However, the most common are three basic MPPT algorithms. The first of these is an algorithm based on the known dependence of the wind turbine power in function of the angular speed $P_G(\omega_m)$ [2,3]. The second one is based on the optimal speed ratio of the λ_{opt} turbine, but it requires the measurement of wind speed [7-10]. The third one is the incremental algorithm, which, without knowing the turbine parameters, continuously searches for operating conditions with maximum power for a given wind speed [11].

At present, AC/DC/AC converters are commonly used in systems with full energy conversion [1,2,3,5]. Until recently, they were implemented on the basis of two-level inverters [2]. Currently, multilevel inverters are used more and more often that place [5]. An increased number of levels allowed them for better shaping of output currents at the same average number of joins of elements. An important feature of circuits with AC/DC/AC converters has become the possibility of their autonomous operation for dedicated recipients. This can be done in the event of power failure from the grid or after the generator is self-excited without the network [3]. Autonomous work is not the subject of the article and will not be discussed here.

2. Model of wind turbine

The induction generators in wind power plants are driven by wind turbines with different rotation axis arrangements. The case modelled in this article refers to the turbine with horizontal axis of rotation. For this turbine, the mechanical power is given by (1).

$$P_m = 0.5\rho A V_w^3 C_p\left(\lambda,\beta\right) = 0.5\rho\pi R_b^2 V_w^3 C_p\left(\lambda,\beta\right) \tag{1}$$

where: $C_p(\lambda,\beta)$ is the wind turbine power coefficient, V_w is the wind speed, and ρ is the air density (assumed $\rho = 1,225$ kg/m³)
The power coefficient $C_p(\lambda,\beta)$ in (1) is given by the empirical relation (2) [7].

$$C_p\left(\lambda,\beta\right) = 0.5176\left(116\lambda_i - 0.4\beta - 5\right)e^{-21\lambda_i} + 0.0068\lambda$$

$$\text{where:}\quad \lambda_i = \frac{1}{\lambda + 0.08\beta} - \frac{0.035}{1+\beta^3} \qquad \lambda = \frac{\omega_T R_b}{V_w} \tag{2}$$

where: λ is the turbine blade tip speed ratio, and β is the turbine blade setting angle, ω_T is the angular speed of the turbine, and R_b is the turbine rotor radius.

In the simulation system, the wind turbine model described above was used to drive an induction generator. For the purposes of simulation tests, the dimensions of turbine blades $R_b = 3$ m and gearbox $G = 5$ were arbitrarily adopted (small wind power plant). The maximal power factor for the adopted model (2) was $C_p(\lambda,\beta) = 0,48$ for $\lambda = 8,1$. The determined values refer to the zero setting angle of the turbine blades $\beta = 0$. Figure 1 shows the turbine power coefficient $C_p(\lambda,\beta)$ for five different turbine blade pitch settings.

However, Figure 2 shows the power of the turbine described above as a function of the angular velocity of the induction generator for different wind speeds with zero blade angle adjustment. The diagram of maximum power is shown on the background of these characteristics This waveform is described in equation (3).

$$a)P_{\max} = c_\beta K \left(\omega_m / G \right)^3 \quad b)c_\beta = \left(\frac{\lambda_{opt0}}{\lambda_{opt\beta}} \right)^3 \frac{C_p \left(\lambda_{opt\beta}, \beta \right)}{C_p \left(\lambda_{opt0}, 0^0 \right)} \quad \text{where} \quad K=0{,}4223 \tag{3}$$
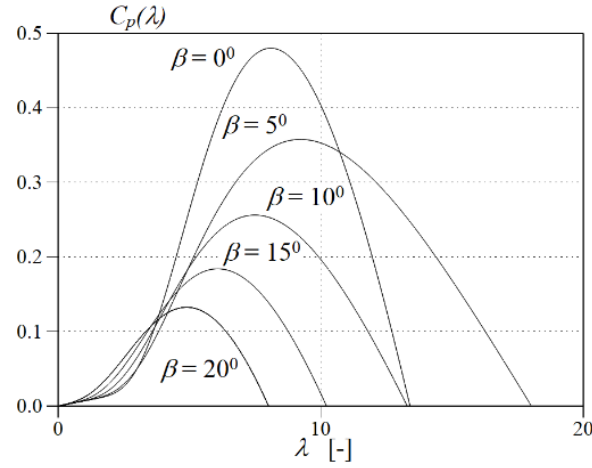

Figure 1. Power coefficient $C_p(\lambda,\beta)$ as a function of the turbine speed ratio for five values of the setting angle.
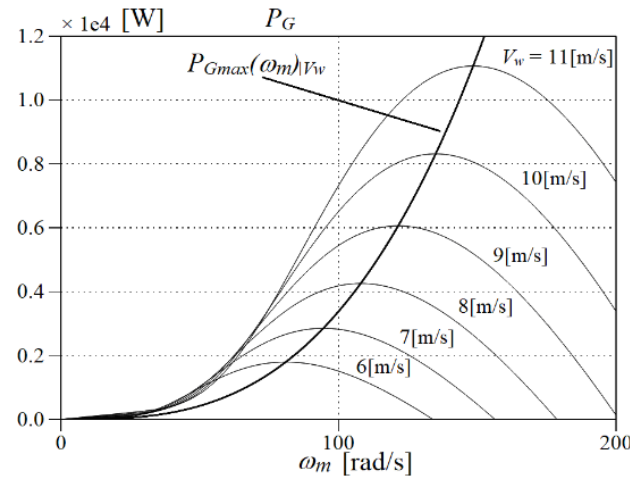

Figure 2. Generator power P_G in relation to the angular speed ω_m for different wind speeds V_w and $\beta = 0^0$.

Equation (3a) for $c_\beta = 1$ describes the generator's maximum power P_{Gmax} for zero adjustment of the blade angle, $\beta = 0$. When the value of power generated exceeds the power rating of the generator P_N, the setting of the angle of the blades changes. To ensure the operation of the generator with the maximum power coefficient $C_p(\lambda,\beta)$ under the new conditions, the coefficient c_β is also changed in accordance with the relation (3b).

Equation (3a) is the basis for the implementation of the Maximum Power Point Tracking method. The tracking method based on the above equation will be used in the further part of the article in simulations of the wind farm system with an induction generator.

3. Multi - level inverters connecting the generator to the power grid

In the connection system of the induction generator to the power grid, three-level inverters were used from both the generator and the power grid side [10]. The types of inverters which were taken into consideration included: Neutral Point Clamped (NPC) inverter, and Neutral Point Piloted (NPP) inverter. Although the NPC inverters contain more elements, they have been accepted for further simulation studies.

In the DC circuit, active balancing of voltage unbalance [10] was applied.

The scheme of a three-level inverter used in simulations on the generator and power grid side, with the active voltage balancing system, is shown in Figure 3.
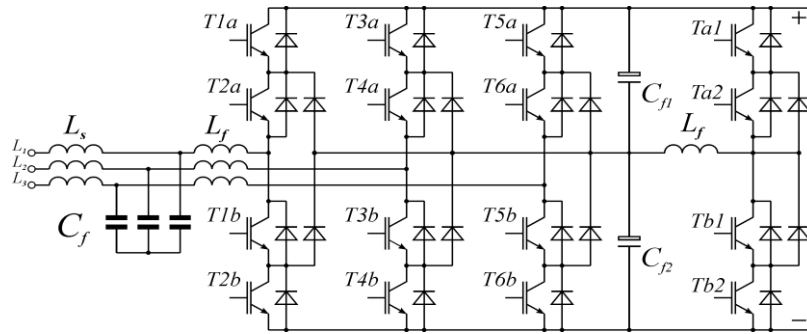

Figure 3. A three-level NPC inverter with autonomic voltage balancing on capacitors C_{f1} and C_{f2}.

4. SPWM modulator of multi - level inverter

A simple algorithm based on sinusoidal pulse width modulation (SPWM) has been used to generate control signals for a multi-level inverter. It is implemented independently for each phase.

At the initial stage, the set signals of phase voltages are modified by adding to them a waveform (4) that allows increasing the output voltage of the inverter.

$$u_{kom} = \frac{\max\left(u_{aref}, u_{bref}, u_{cref}\right) + \min\left(u_{aref}, u_{bref}, u_{cref}\right)}{2}$$
$$u_{xref} = u_{xref} - u_{kom} \qquad x = a, b, c \tag{4}$$

The obtained modified signals are compressed to a range of ±2 using the U_{DC} intermediate circuit voltage (5).

$$u_x = 2 \frac{u_{xref}}{U_{DC}} \qquad x = a, b, c \tag{5}$$

In the next processing step, the signals were shifted by adding a constant component to them with a value of 2. As a result of this operation, unipolar signals in the range of values from 0 to 4 (6) were obtained.

$$u_{px} = u_x + 2 \qquad x = a, b, c \tag{6}$$

Signals processed this way are analyzed in two ranges, in the range of values 0-2 and 2-4. In each of these intervals, the SPWM modulation is implemented independently. In the range of values from 2-4, signals are generated for the upper transistors of each inverter branch *T1a, T3a, T5a* and in the range of values from 0-2 for the lower transistors *T2a, T4a, T6a*. The other inverter transistors are controlled by complementary signals *T1b, T3b, T5b* and *T2a, T4a, T6a* according to Figure 3.

The durations of the control signals for a single switching cycle of the transistors are calculated twice in advance of the half cycle after the prediction has been applied to the set signals. They are performed at the beginning and in the middle of the switching cycle. The control signals obtained in this way may be asymmetrical with respect to the center of the switching cycle. The implementation of the control described above, however, halves the delay in the system response to changes in the set point and load in relation to the single calculation of the signal duration only at the beginning of the switching cycle.

Simple mathematical relations, without trigonometric functions, significantly reduced the calculation time. In the initial phase, the implementation of the algorithm was

limited to determining the range of the offset value of the set signal. The calculation procedure is started only after the preparation phase. In the case when the value of the set point signal was in the second range, the initial offset value should be subtracted before making the calculation. This operation is not required when the signal value is in the first range (7).

$$u_{rx} = \begin{cases} u_{px} - 2 & 2 < u_{px} < 4 \\ u_{px} & 0 < u_{px} < 2 \end{cases} \qquad x = a,b,c \tag{7}$$

Eventually, the calculation of the delay times of the switching signals of the transistors, in relation to the beginning and the middle of the switching cycle, are performed based on dependencies (8).

$$T_a = \left(1 - 0.5u_{rx}\right)T_p \qquad x = a,b,c \tag{8}$$

where: T_p is the half of the interval T_{PWM}, and u_{rx} is the reduced value of the set voltage

The switching delay time determined on the basis of the above dependence applies only to one transistor from the complementary pair in the phase. At that time, the transistor from the second complementary pair can be switched on for the time equal to half of the connection cycle (second interval) or off for the time equal to half of the connection cycle (first interval) (9). It depends on the actual value of the set signal.

$$\begin{bmatrix} T_{xi} \\ T_{x(i+1)} \end{bmatrix} = \begin{cases} \begin{matrix} \left(1 - 0.5u_{rx}\right)T_p \\ 0 \end{matrix} & 2 < u_{px} < 4 \\ \begin{matrix} T_p \\ \left(1 - 0.5u_{rx}\right)T_p \end{matrix} & 0 < u_{px} < 2 \end{cases} \tag{9}$$
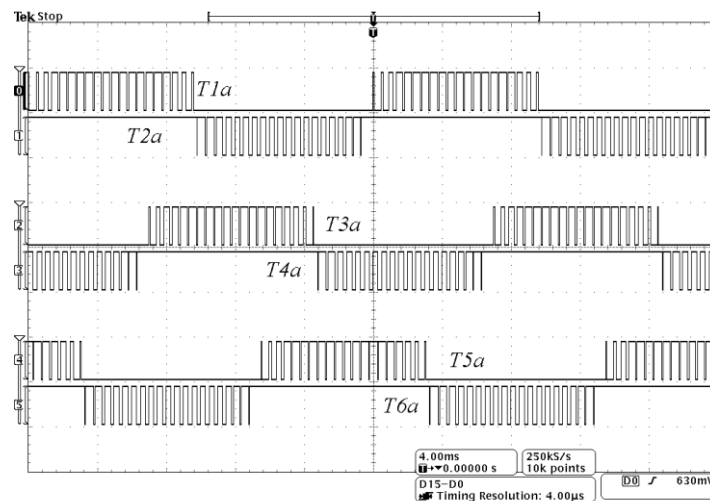
where: $[x,i] \in <a,1;b,3;c,5>$

Figure 4. Control signals based on the proposed algorithm (experiment).

Figure 4 shows the waveforms of transistor control signals realized using the presented algorithm. They present the determined operating state of the three-level inverter.
The above algorithm can be easily adapted for controlling the operation of inverters with a larger number of levels.

5. Field-oriented generator control with direct orientation of the vector (DFOC)

In the power plant system, the generator is a squirrel cage induction machine with the rated data in the Appendix.

Direct coupling of such a generator with the power grid is possible, but only in a very narrow range of angular velocities. In order to extend the speed range for which the generator will be able to supply energy to the power grid, a solution with full conversion based on the AC/DC/AC system was used. It forced the necessity of using the converter also on the generator side. In order to unify control systems and create the possibility of using medium voltage generators in the future, three-level inverters were used.

The generator-side inverter control algorithm was based on field-oriented control with indirect field vector orientation with voltage control. It is relatively simple and allows setting the electromagnetic moment of the generator load. This is the starting point for the implementation of the MPPT algorithm. The cage induction motor model in the synchronous system of the rotor flux is described by the voltage-current vector equation (10). After separation into the real and imaginary part, it allows to determine the rotor flux ψ_r, the slip pulsation ω_r and the electromagnetic torque m_e (11).

$$T_r \frac{d\vec{\psi}_r}{dt} + \left(1 + jT_r\omega_r\right)\vec{\psi}_r = L_m\vec{i}_{fG} \qquad T_r = \frac{L_r}{R_r} \tag{10}$$

$$\omega_r = R_r \frac{L_m}{L_r} \frac{i_{fq}}{|\psi_r|} \qquad \gamma_{\psi r} = \int_0^t \left(p_b\omega_m + \omega_r\right)dt$$

$$T_r \frac{d\psi_r}{dt} + \psi_r = L_m i_{fd} \qquad m_e = \frac{3}{2} p_b \frac{L_m}{L_r} |\psi_r| i_{fq} \tag{11}$$

where: R_r rotor resistance, L_r rotor inductance, L_m main inductance, p_b number of pole pairs, ψ_r rotor flux, ω_r slip pulsation, ω_m mechanical angular velocity, m_e torque

Equations (11) describe the induction machine in synchronous system. They also make it possible to calculate the set component values i_{fd}^*, i_{fq}^* of the inverter output current. These current components were calculated for the assumed value ψ_r^* of the rotor flux and the set value m_e^* of the electromagnetic torque. To enable wider use of the machine as the generator, the rotor flux was assumed equal to the rated flux. On the other hand, the set moment was calculated in MPPT system, based on the current angular speed ω_m of the generator shaft. As a result of such procedure, relations (12) were obtained. They allowed to determine the inverter control in a further calculation step.

$$\omega_r[k] = R_r \frac{L_m}{L_r} \frac{i_{fq}[k]}{|\psi_r[k]|} \qquad \omega_{s\psi r}[k+1] = p_b\omega_m[k] + \omega_r[k]$$

$$\gamma_{\psi r}[k+1] = \gamma_{\psi r}[k] + T_s\omega_{s\psi r}[k]$$

$$m_e[k] = \frac{3}{2} p_b \frac{L_m}{L_r} \psi_r[k]i_{fq}[k] \tag{12}$$

$$\psi_r[k+1] = \psi_r[k] + T_s/T_r\left(L_m i_{fd}[k] - \psi_r[k]\right)$$

Figure 5. shows the inverter control algorithm from the generator side using the method based on dependence (12).

$$i_{fd}^*[k] = K_{P\_\psi_r}\left[\left(\psi_r^*[k] - \psi_r[k]\right)\right]$$

$$+ K_{I\_\psi_r} \sum_{m=0}^{k}\left[\left(\psi_r^*[m] - \psi_r[m]\right)\right]$$

$$i_{fq}^*[k] = K_{P\_me}\left[\left(m_e^*[k] - m_e[k]\right)\right] \tag{13}$$

$$+ K_{I\_me} \sum_{m=0}^{k}\left[\left(m_e^*[k] - m_e[k]\right)\right]$$

In the presented block diagram, the generator is controlled in a coordinate system that rotates synchronously with the rotor flux vector ψ_r. Here, on the basis of the set values

of the rotor flux $\psi_r{}^*$ and the motor torque $m_e{}^*$, the set currents $i_{fd}{}^*$ and $i_{fq}{}^*$ in the d-q axes are determined by means of PI type controllers (eq. 13). Next, on the basis of the set values of currents $i_{fd}{}^*$ and $i_{fq}{}^*$, the set values of the output voltages $u_{fd}{}^*$ and $u_{fq}{}^*$ of the converter are determined also by means of PI type regulators (eq. 14).

$$
\begin{aligned}
u_{fd}{}^*[k] = K_{P\_i_{fd}} &\left[\left(i_{fd}{}^*[k] - i_{fd}[k] \right) \right] \\
&+ K_{I\_i_{fd}} \sum_{m=0}^{k} \left[\left(i_{fd}{}^*[m] - i_{fd}[m] \right) \right] \\
u_{fq}{}^*[k] = K_{P\_i_{fq}} &\left[\left(i_{fq}{}^*[k] - i_{fq}[k] \right) \right] \\
&+ K_{I\_i_{fq}} \sum_{m=0}^{k} \left[\left(i_{fq}{}^*[k] - i_{fq}[k] \right) \right]
\end{aligned}
\tag{14}
$$
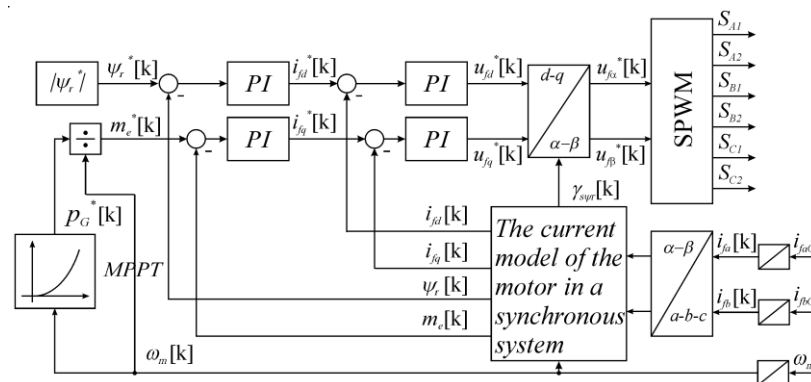
Figure 5. Block diagram of the induction generator control algorithm.

6. Control of the power grid converter

The AC/DC/AC system's output converter works with the power grid directly. Its basic task is to supply energy generated by the generator to the grid. Thanks to the extended control algorithm, it can also act as a reactive power compensator.

In general, the grid voltage can be strongly distorted and contain higher harmonics with significant amplitudes. In the simulation tests, two harmonics were taken into account: 5h with a value of 5% of the fundamental value of the harmonic and phase 30⁰ and 7h with a value of 3% of the fundamental value of the harmonic and phase of -20⁰. The condition of proper cooperation with the power grid is a good synchronization of the control system with the basic voltage harmonic. This goal was achieved using the PLL algorithm. However, when the network voltage is distorted, good synchronisation is not sufficient to obtain the nearly sinusoidal voltage waveform with small content of higher harmonics. In order to perform the above task, the LCL filter was used in the inverter coupling system with the power grid, and the prediction in the control algorithm was applied [16-23]. The use of the filter in conjunction with the prediction has improved the shape of the grid current by reducing the content of higher harmonics below 1%.

The equivalent filter scheme is shown in Figure 6. It has a high damping factor of 60 dB/dec for frequencies above the resonant frequency. By appropriate selection of the resonant frequency, the modulation signal can be very effectively suppressed. However, it is a third-order filter and oscillations may occur in the output current, which must also be effectively suppressed.

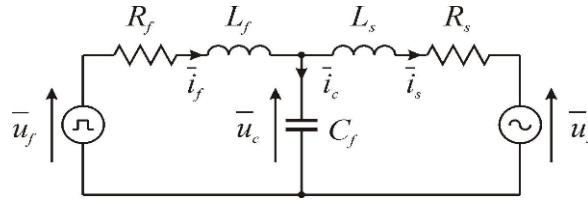Equations (15 abc) describe the LCL filter in a continuous form.

Figure 6. Equivalent LCL coupling filter scheme.

$$\text{a)} \quad L_s \frac{d\vec{i_s}}{dt} + \vec{i_s} R_s = \vec{u_c} - \vec{u_s} \quad \text{b)} \quad L_f \frac{d\vec{i_f}}{dt} + \vec{i_f} R_f = \vec{u_f} - \vec{u_c}$$
$$\text{c)} \quad C_f \frac{d\vec{u_c}}{dt} = \vec{i_s} - \vec{i_f} \tag{15}$$

When switching to a discrete form, a description based on averaged momentary values of the grid voltage, inverter and capacitor was used. Finally, the predictive control algorithm with the model was described using four vector equations (16) [11].

$$\vec{u_f}[k+1\,|\,k+2] = \vec{u_c}[k+1\,|\,k+2]$$
$$+\left(\vec{i_f}[k+2] - A_f * \vec{i_f}[k+1]\right)/B_f$$
$$\vec{i_f}[k+2] = \vec{i_s}[k+2] + \left(\vec{u_c}[k+2\,|\,k+3]\right.$$
$$\left. - A_f * \vec{u_c}[k+1\,|\,k+2]\right)/B_f$$
$$\vec{u_c}[k+2\,|\,k+3] = \vec{u_s}[k+2\,|\,k+3]$$
$$+\left(\vec{i_s}[k+3] - A_s * \vec{i_s}[k+2]\right)/B_s \tag{16}$$
$$\vec{u_c}[k+1\,|\,k+2] = A_c * \vec{u_c}[k\,|\,k+1]$$
$$+B_c * \left(\vec{i_f}[k+1] - \vec{i_s}[k+1]\right)$$

where: x[k+1|k+2] average value of the quantity in the time interval k+1 to k+2, x[k+1] value of the quantity at time k+1

For a third-order filter, the prediction of two advance steps is required. In order to implement the control in the above equations, the grid current values were replaced with theirset values: $\vec{i_s}[k+2] = \vec{i_s^*}[k+2]$ and $\vec{i_s}[k+3] = \vec{i_s^*}[k+3]$. The remaining values were determined based on equation (17).

$$\vec{u_c}[k-1\,|\,k] = \vec{u_s}[k-1\,|\,k] + \left(\vec{i_s}[k] - A_s * \vec{i_s}[k-1]\right)/B_s$$
$$\vec{u_c}[k\,|\,k+1] = A_c * \vec{u_c}[k-1\,|\,k] + B_c * \left(\vec{i_f}[k] - \vec{i_s}[k]\right)$$
$$\vec{i_s}[k+1] = A_s * \vec{i_s}[k] + B_s * \left(\vec{u_c}[k\,|\,k+1] - \vec{u_s}[k\,|\,k+1]\right)$$
$$\vec{i_f}[k+1] = A_f * \vec{i_f}[k] + B_f * \left(\vec{u_f}[k\,|\,k+1] - \vec{u_c}[k\,|\,k+1]\right) \tag{17}$$

In the grid converter control system, the voltages on the capacitors and the converter output currents are not measured. However, these values are calculated. The average voltages $\vec{u_c}[k-1\,|\,k]$ on the capacitors for the previous sampling period are estimated on the basis of the average values of the power grid voltage and the grid current in the previous sampling period. Then, based on the prediction, its values for the present moment are determined. In contrast, the converter output currents are calculated based on the prediction in the previous sampling period. The coefficients occurring in the equations (17) were determined based on the equations of the filter state and assuming the constancy of the element parameters, they can be calculated based on the dependence (18).

$$A_s = 1 - \exp(-T_s/T_e) \qquad B_s = (1 - A_s)/R_s$$
$$A_f = 1 - \exp(-T_s/T_f) \qquad B_f = (1 - A_f)/R_f$$
$$A_c = 1 - \exp(-T_s/T_c) \qquad B_c = (1 - A_c) * R_c \qquad (18)$$
$$T_e = L_s/R_s \qquad T_f = L_f/R_f \qquad T_c = C_f R_c$$

In equations (16,17), the average grid voltage was used for the intervals [k|k+1], [k+1|k+2] and [k+2|k+3] and the currents from the moment of measurement [k]. The averaging refers to half of the switching cycle of transistors. The coefficients in the equations include such parameters of the coupling system as the filter inductances L_s and L_f, filter resistances R_s and R_f, as well as capacitance C_f and resistance R_c = ESR.

The voltage values of the power grid at the time [k+1], [k+2] and [k+3] were determined by summing (21) rotated vectors, basic (19) and higher harmonics (20), grid voltage. On the other hand, the size of the rotation angle of the vector components depends on their pulsation ω_{Pll1h}, ω_{mh} and sampling time T_s.

$$\vec{u}_{sPll1h}[k+n] = \vec{u}_{sPll1h}[k]\left(\cos\left(nd\gamma_{Pll1h}\right) + j\sin\left(nd\gamma_{Pll1h}\right)\right)$$
$$\text{where: } d\gamma_{Pll1h} = 2PIf_{Pll1h}T_s \quad n = 1, \ 2, \ 3 \qquad (19)$$

$$\vec{u}_{smh}[k+n] = \vec{u}_{smh}[k]\left(\cos\left(nd\gamma_{mh}\right) + j\sin\left(nd\gamma_{mh}\right)\right)$$
$$\text{where: } d\gamma_{mh} = 2PIf_{mh}T_s \quad m = 5, \ 7,... \ n = 1, \ 2, \ 3 \qquad (20)$$

$$\vec{u}_s[k+n] = \vec{u}_{sPll1h}[k+n] + \sum_m \vec{u}_{smh}[k+n]$$
$$\text{where: } n = 1, \ 2, \ 3 \ m = 5, \ 7,... \qquad (21)$$

The components of the current $i_{s\alpha\beta}$ and $i_{f\alpha\beta}$ for time [k+1] (17) are determined based on prediction with the model of coupling circuit, Figure 6.

The set value of the current was determined based on the definition of instantaneous powers for the first harmonic, given by Hirofumi Akagi (22) [14,15].

$$p^*[k] = u_{s\alpha Pll1h}[k]i_{s\alpha}^*[k] + u_{s\beta Pll1h}[k]i_{s\beta}^*[k]$$
$$q^*[k] = u_{s\beta Pll1h}[k]i_{s\alpha}^*[k] - u_{s\alpha Pll1h}[k]i_{s\beta}^*[k] \qquad (22)$$

It refers to the actual time [k]. However, in relations (16), values of currents are also required for times [k+2] and [k+3]. Assuming that the power grid current should have the sinusoidal waveform, the required quantities can be easily obtained. For this purpose, it is carried out twice and three times the rotation of the reference current vector, determined for the instant [k] based on the dependence (22), by the angle determined from the fundamental harmonic voltage of the power grid frequency f_{Pll1h} of network voltage and the sampling interval T_s (23).

$$\vec{i}_s^*[k+n] = \vec{i}_s^*[k]\left(\cos(n * d\gamma_{Pll1h}) + j\sin(n * d\gamma_{Pll1h})\right)$$
$$\text{where: } d\gamma_{Pll1h} = 2PIf_{Pll1h}T_s \qquad n = 2, \ 3 \qquad (23)$$

Figure 7. shows a block diagram of the grid converter control algorithm based on the presented dependencies.

7. Synchronization of control to the voltage of the power grid

As mentioned earlier, the control of the converter, which is connected to the power grid, requires precise synchronization with the voltage waveform. In the presented system, this process takes place in two stages. In the first stage, thirty-two positive order and
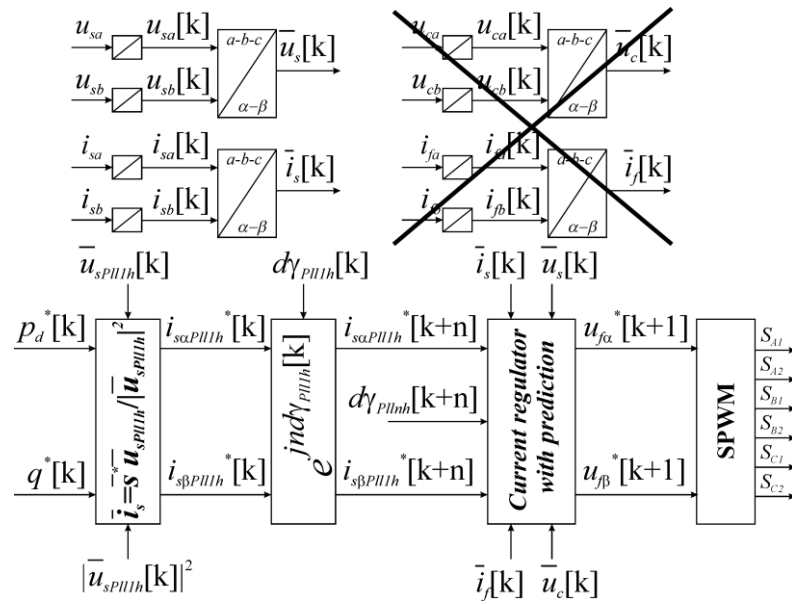
Figure 7. Block diagram of the grid converter control algorithm.

thirty-two negative order higher harmonics are attenuated using a cascaded system $CDSC(v_{\alpha\beta})_{2,4,8,16,32,64}$. [24-28]. A valuable feature of this system is that it does not introduce, or introduces a negligibly small value of, phase shift of the input waveform first harmonic.

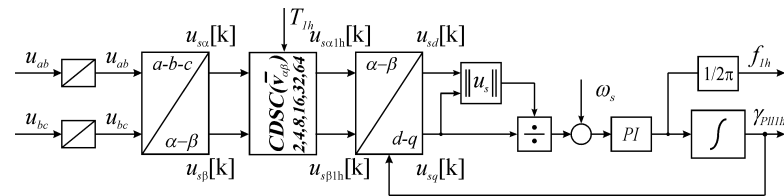The second stage is proper synchronization with the fundamental harmonic of the power grid voltage. Figure 8 shows the implemented synchronization system.

Figure 8. Block diagram of CDSC – PLL system.

8. Wind power plant system

Figure 9 shows a complete block diagram of a wind power plant connected to the power grid by three-level inverters. The connection between the power plant and the power grid is constituted by an LCL filter with the parameters given in the Appendix. In the DC circuit there is a voltage balancing system on capacitors C_{f1} and C_{f2}. Between the control systems: generator and power grid inverter, feed-forward power coupling has been used. It speeds up the transient processes in the converter system at rapid changes in wind speed.

9. Laboratory tests of a wind power plant

The tests of the system were carried out by simulation using the software package PLECS in version 4.4.3, and the limited physical experiment. From this package, only library elements of the main circuit were used for modelling. These elements include: model of induction motor, transistors, inductances, and capacitances, as well as current, voltage, and speed measurement systems. The control algorithm was written in the C programming language. After compiling, in the form of a dynamic library *.dll, it was attached to the main program modeling system. The control algorithm is called from the main program every 50 μs (20 kHz) similarly as it is done in the real system as part of the interrupt service. However, the frequency of switching of transistor keys is by half and in the tested system it is 10 kHz.
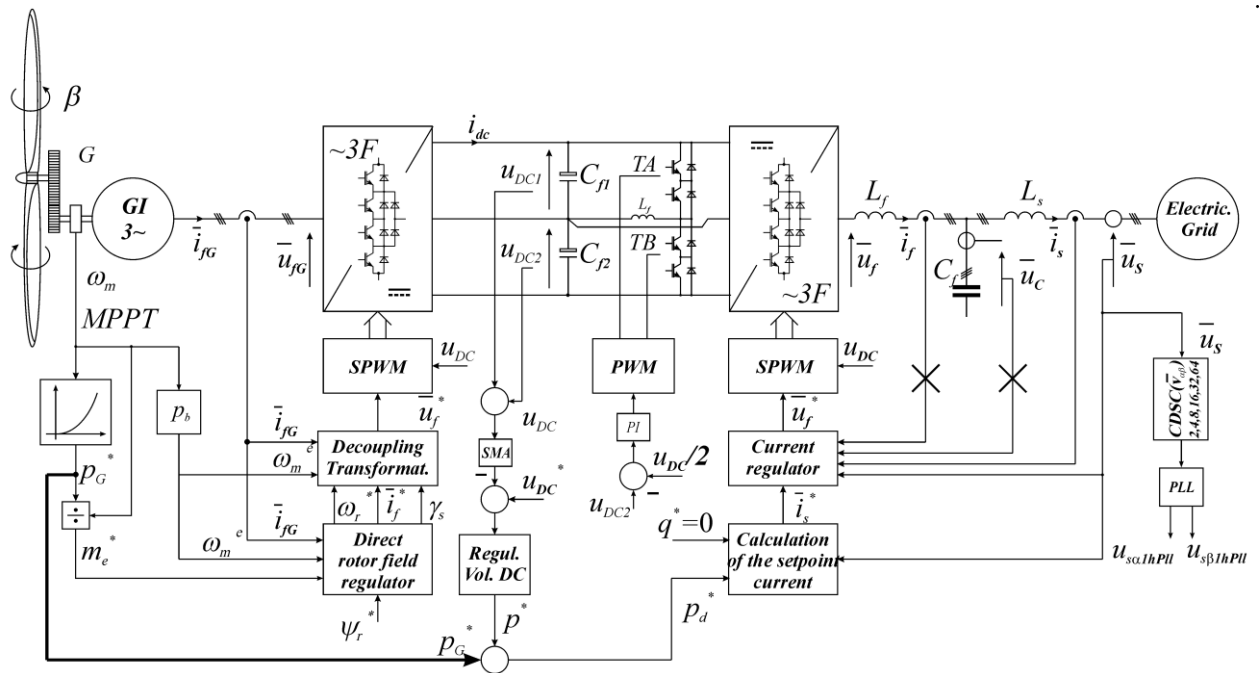
Figure 9. Wind power plant with an induction generator and AC/DC/AC converter based on three-level inverters.

The procedure presented above was dictated by the fact that in the case of experimental implementation, the tested algorithm can be easily transferred to a microprocessor controller with minor modifications to adapt it to the hardware equipment. The laboratory research process carried out in this way will reproduce the working conditions of the real system fairly reliably.
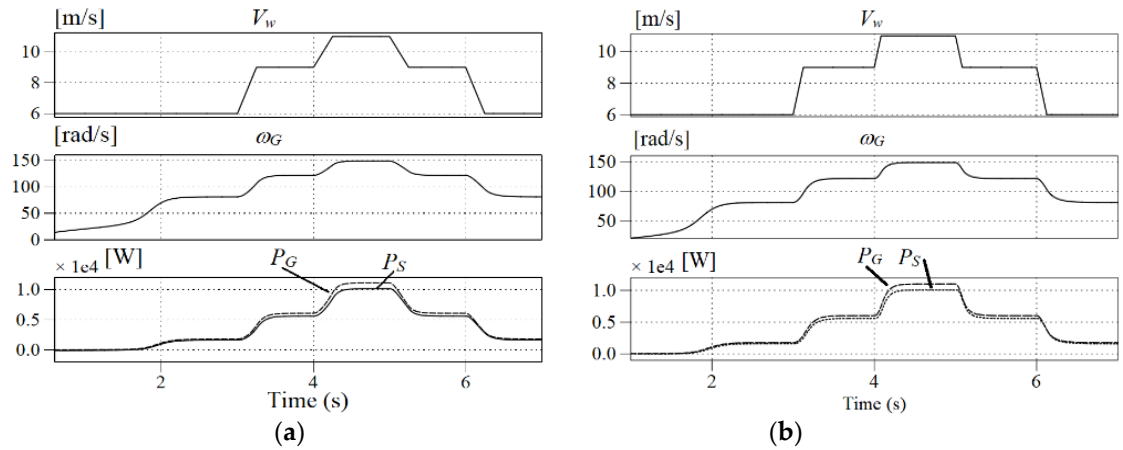

Figure 10. Assumed changes in wind speed V_w (**a**) 12, 8, -8, -12 [m/s²]; (**b**) 24, 24, -24 -24 [m/s²] and corresponding changes in angular velocity ω_G, generator power P_G and power grid P_S.

During the simulation tests, the wind was modeled changing in the cycle from 6 m/s to 9 m/s and further to 11 m/s and from 11 m/s to 9 m/s finishing at 6 m/s with phases of constant speed value. The operation of the system for the above test scenario is given in Fig. 10, which shows the assumed changes of wind speed V_w and the corresponding changes of angular speed ω_G and power P_G of the generator, as well as of power P_S supplied to the power grid.

Figure 11a shows the waveforms of generator power P_G as function of its angular speed ω_G, while Fig. 11b presents the waveform of wind turbine power coefficient $C_p(\lambda,\beta)$. These two waveforms were obtained for different wind speeds at a constant turbine blade pitch $\beta = 0^0$. Power values at which changes start, after changes in wind speed, allow to

conclude on the good implementation of the maximum power point tracking in steady states.
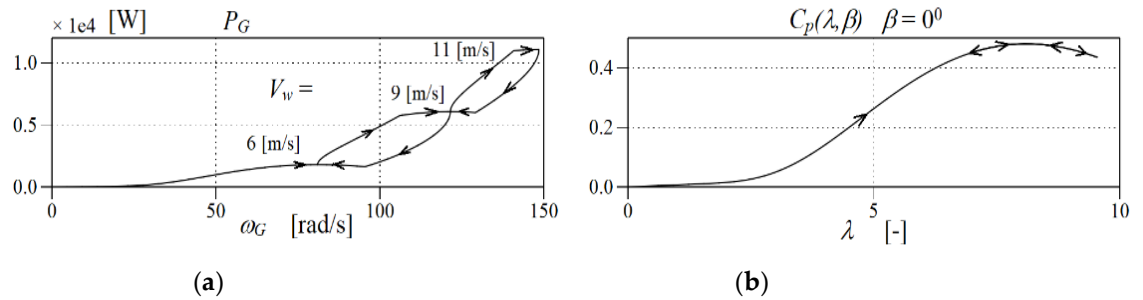

Figure 11. Waveforms of generator power P_G (**a**) and turbine power coefficient $C_p(\lambda,\beta)$ (**b**) for changing wind speed V_w and blade angle equal to $\beta = 0^0$.

Figures 12 and 13 show changes in wind speed V_w, angular speed ω_G and power of generator P_G as well as of power P_S supplied to the power grid. The presented waveforms refer to the case of wind speed increase from 9 m/s through 12 m/s up to 14 m/s, and the decrease within the same range. When the wind speed exceeded 11 m/s, the generated power was higher than the rated power of the generator. In order to limit the power, the angle of the wind turbine blades setting was changed from $\beta = 0^0$ to $\beta = 10^0$ to reduce the generated power. Despite this change, the wind power plant continues to work with the tracking of the maximum power point by correcting the coefficient c_β in accordance with the equation 3b. On the basis of the waveform Figure 10 determined the efficiency of the system, which, for a predetermined wind velocity $V_w = 11$ m/s and an angle $\beta = 0^0$ was $\eta \cong 91,2\%$.

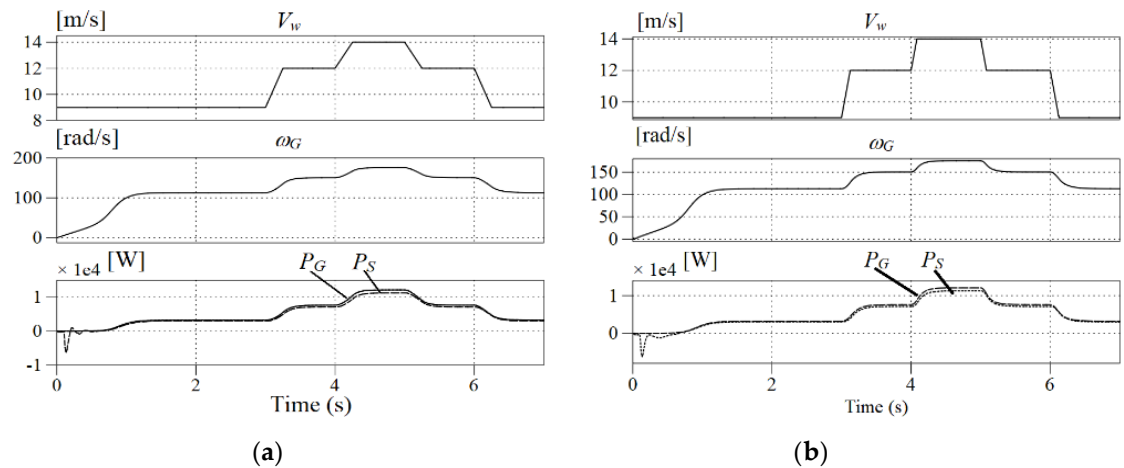**Figure 12.** Waveforms of wind speed V_w (**a**) 12, 8, -8, -12 [m/s²] (**b**) 24, 24, -24 -24 [m/s²] generator angular speed ω_G and power P_G, and grid power P_S, for $\beta = 10^0$.
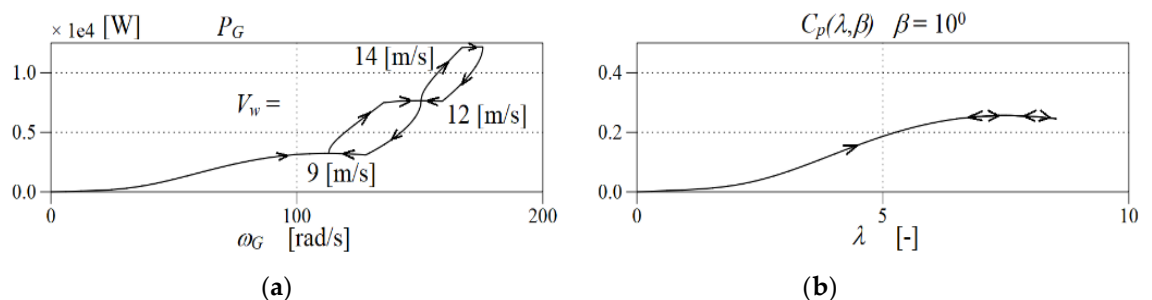

Figure 13. Waveforms of generator power P_G (a) and turbine power coefficient $C_p(\lambda,\beta)$ (b) for changing wind speed V_w and blade angle equal to $\beta = 10^0$.

Figures 14 and 15 show the transient processes occurring in a wind power plant during a linear change of the turbine blade angle setting in the range from $\beta = 0^0$ to $\beta = 15^0$, at constant wind speed. In the initial phase of changes of β, a slight increase of generator angular speed ω_G is observed, but then it decreases to the final steady-state level below the initial speed. As a result, the power factor $C_p (\lambda,\beta)$ decreases (Figure 15b) from the optimum value for the set wind speed $V_w = 11$ m/s and angle $\beta = 0^0$ to the optimal value for the angle $\beta = 15^0$. Therefore, the power P_G generated and P_S supplied to the power grid is also decreasing (Figure 14, 15a).
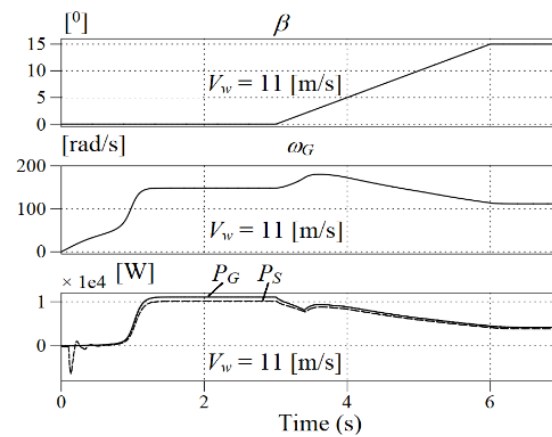

Figure 14. The waveforms of the angle of the wind turbine blades β, the angular velocity ω_G, the power P_G and supplied to the power grid P_S.

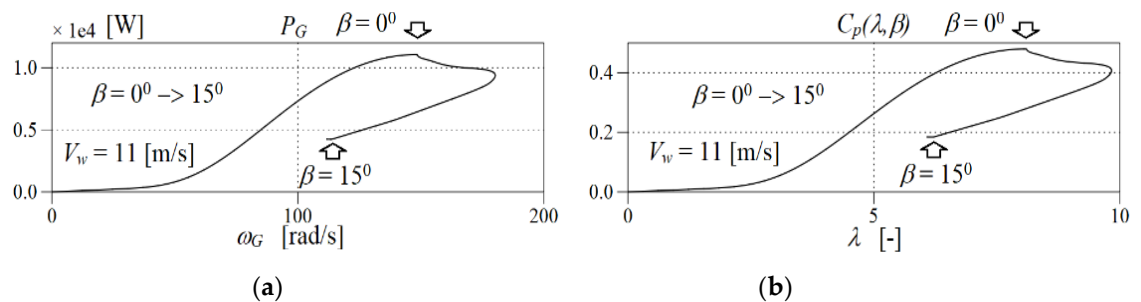(a)   (b)

Figure 15. Waveforms of generator power P_G (**a**) and turbine power coefficient $C_p(\lambda,\beta)$ (**b**) for constant wind speed and blade setting angle β changing from 0^0 to 15^0.

Figure 16 shows voltage u_{abG} and current i_{aG} waveforms on the generator inverter side. The waveforms on the left refer to the change in wind speed in the range from 6 to 9 m/s, while on the right side the wind speed varies from 9 to 6 m/s. The center waveforms show the steady state of the generator at wind speed of 11 m/s. Despite the wide range of wind speed variations, the converter work is correct. The converter passes without disturbance to the three-level mode when the wind speed increases and vice versa to the two-level mode while reducing the wind speed. The obtained waveforms indicate the correct operation of the system in various conditions.

The proposed simplified algorithm of the three-level inverter modulator works correctly. This is confirmed by the simulation results obtained. Switching processes of transistors are ordered and there is no uncontrolled switching in them as evidenced by voltage waveforms.

In all of the above cases, the generator current is close to sinusoidal with a low content of higher harmonics (Figure 16). Higher harmonics generating pulsating torque and increase the loss of induction generator so their lack of positive effect on the system.

Figure 17a shows the setpoints and measured quantities in the direct control system for the rotor flux and electromagnetic torque of on induction generator. Figure 18b, on the

other hand, shows the corresponding setpoints and measured values of the stator current components in a coordinate system rotating synchronously with the rotor flux.
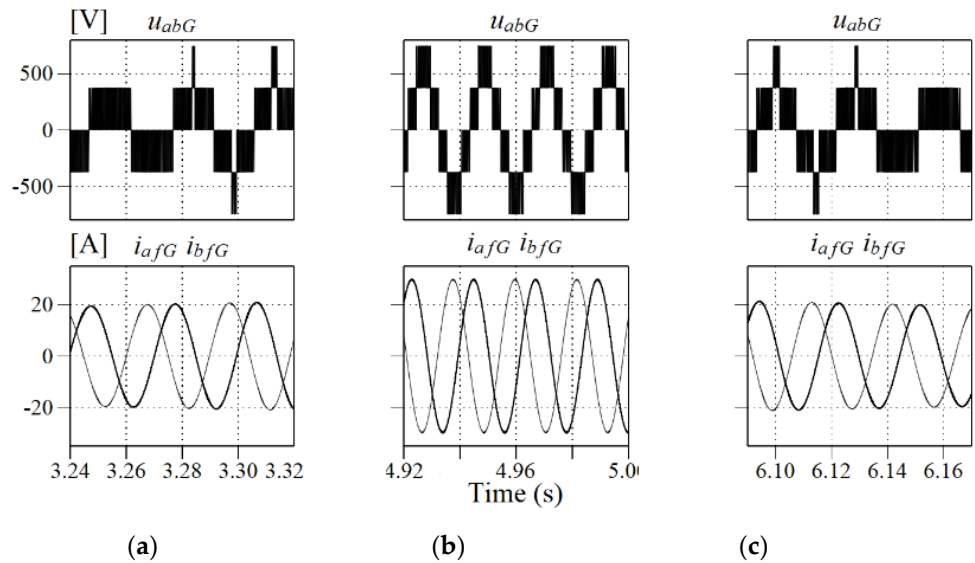

Figure 16. Waveforms of generator voltage u_{abG}, and currents i_{afG}, i_{bfG} at changing (**a**), (**c**) and constant wind speed equal to 11 m/s (**b**).

Figure 17a shows the setpoints and measured quantities in the direct control system for the rotor flux and electromagnetic torque of on induction generator. Figure 18b, on the other hand, shows the corresponding setpoints and measured values of the stator current components in a coordinate system rotating synchronously with the rotor flux.
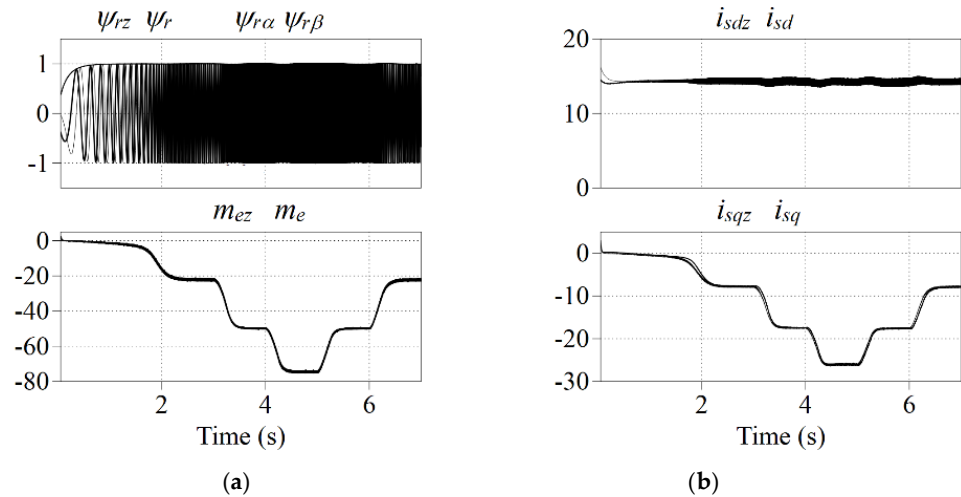

Figure 17. The waveforms of: (**a**) the set rotor flux ψ_{rz}, the set driving torque of a wind turbine m_{ez} and estimated values ψ_r and electromagnetic torque of generator m_e (**b**) the set current components in the d and q axes and their measured values.

Figure 18 shows the voltage waveforms u_{abf} of the converter connecting the system to the power grid, the power of the induction generator P_G, power supplied to the power grid P_S and reactive power Q_S. In the lower part of the figure shows the waveform of the power grid current i_{as} and the output current of the inverter i_{af}. The waveforms were obtained during the sequence of wind speed changes from 6 m/s by 9 m/s to 11 m/s and in the opposite direction of changes ending with the wind speed of 6 m/s.

On the waveforms, an increase in the current can be observed at the moment of setting reactive power. Figure 19 shows in detail the steady state of the power plant operation at a wind speed of 11 m/s with a load determined from the operation of the MPPT system.

To fully illustrate the system's capabilities at time t= 4,6s, the reactive power of $Q_S = 5$ kVar was applied to the grid converter control system (Figure 18). This caused temporary additional switching of the inverter transistors. They are clearly visible on the output waveform of the u_{abf} inverter (Figure 19). They cause immediate displacement of the i_{as} current grid phase (Figure 19). However, a fast change of the output current phase does not lead to oscillations. Thanks to the use of advanced control, it was possible to avoid unfavorable oscillation phenomena in the output current of the multi-level inverter.
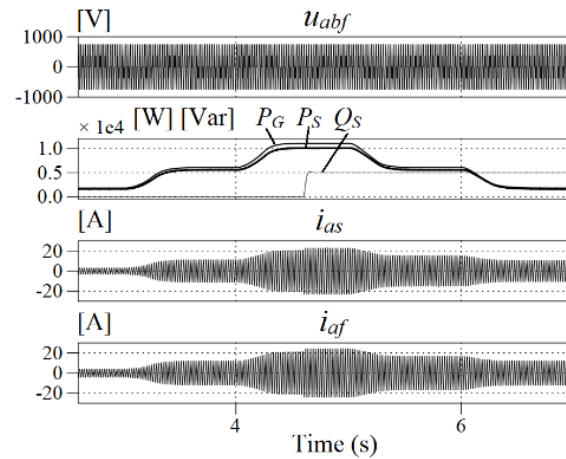

Figure 18. Waveforms of the generator's phase-to-phase voltage u_{abf}, power output P_G, power supplied to the grid P_S, reactive power Q_S, grid current i_{as} and inverter current i_{af}.
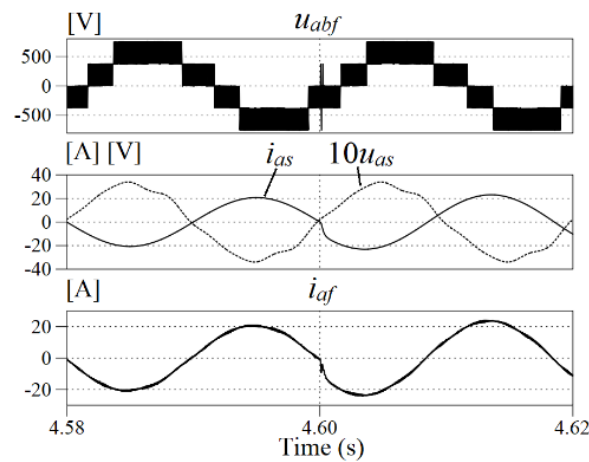

Figure 19. Waveforms of the phase-to-phase voltage of the power grid inverter u_{abf}, voltage u_{as} and current i_{as} of the grid and inverter current i_{af} for change of reactive power.

Despite the strong distortion of the power grid voltage, which contains 5h with a value of 5% and 7h with a value of 3% of the fundamental value of the harmonic, the current waveform i_{as} is close to sinusoidal with the content of higher harmonics below 1% (Table 1).The content of higher harmonics of the power grid current has not changed much with the changes of load and type of control. (where: f_G - generator voltage frequency)

In the presented waveforms, the correct operation of the proposed simplified modulators can be observed also in the case of a converter connected to the power grid (Figure 19). Lack of asymmetry of the output voltages three-level inverter proves the proper operation of the balancing voltage in the DC voltage circuit

Figure 20 shows the voltage and current waveforms after connecting the system to the power grid. In spite of the strongly deformed voltage waveform, the obtained current is close to sinusoidal.

Table 1. The content of higher harmonics.

Type of system	P_s [kW]	f_G [Hz]	Content of higher harmonics			
			THD_I_G%	THD_U_S%	THD_I_f%	THD_I_S%
With all	5.5	37.39	0.83	5.83	5.26	0.18
measurements	10.0	45.40	0.61	5.76	2.68	0.05
Without	5.5	37.41	0.83	5.83	5.29	0.18
measurement u_c	10.0	45.40	0.61	5.83	2.68	0.05
Without	5.5	37.39	0.83	5.83	-	0.695
measurement u_c, i_f	10.0	45.40	0.61	5.83	-	0.37
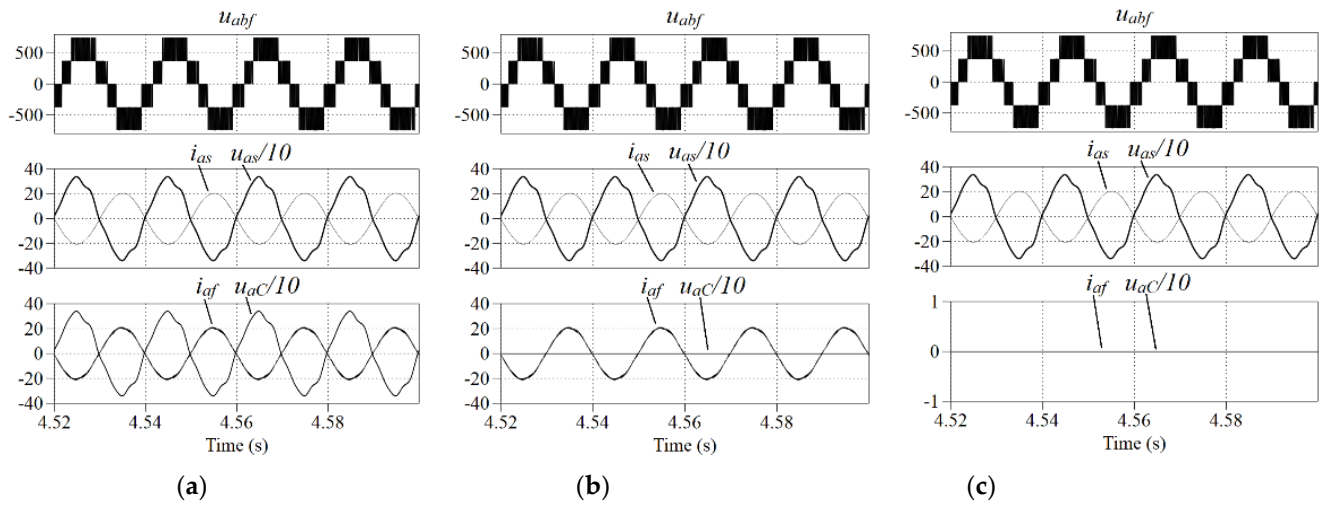
Figure 20. Voltage waveforms u_{abf} and current i_{af} of the inverter, u_{abs} voltage and current i_{as} of the power grid and u_{aC} capacitor voltage in steady state (**a**) with all measurements (**b**) without measuring the capacitor voltage (**c**) without measuring the inverter current and capacitor voltage.

Based on the simulation tests performed, the correct operation of the small wind power plant system was observed. The power plant's control algorithm efficiently tracks the point of maximum power, both in the case of changes in wind speed and changes in the angle of setting the wind turbine blades.

Figure 21a, b shows the experimental and simulation results of the simplified modulator realizing the set value of the output voltage of the three-level inverter without the use of arrays and trigonometric functions. Figure 22, on the other hand, documents the sinusoidal waveform of the grid current despite the strong distortion of its voltage.
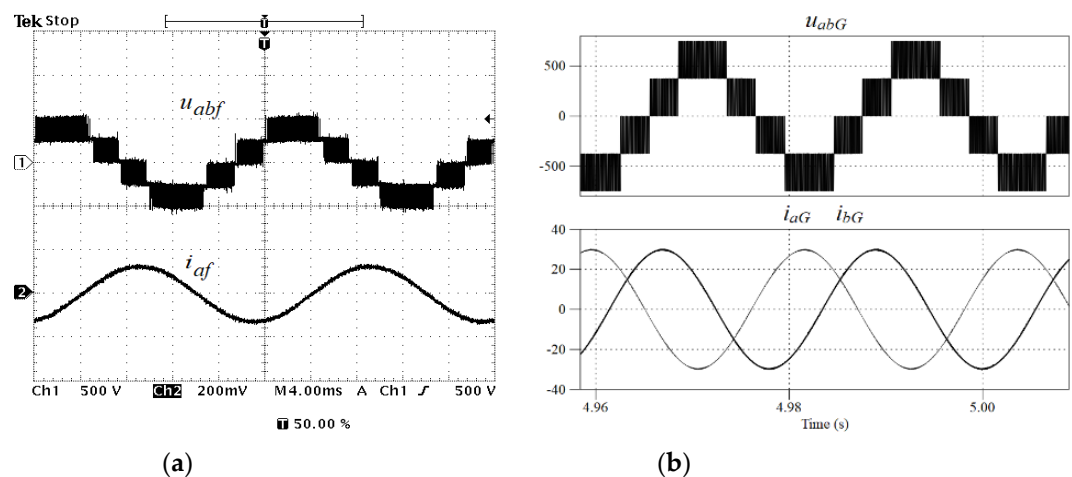
Figure 21. Voltage u_{abf} and current i_{af} waveforms (**a**) experiment (**b**) simulation.
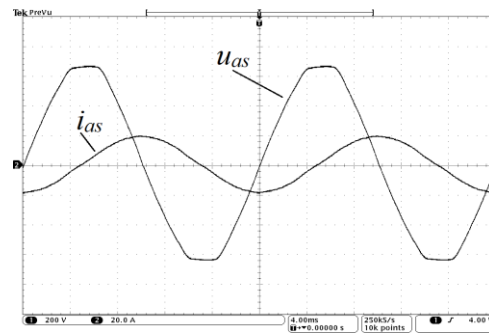
Figure 22. Voltage u_{as} and current i_{as} waveforms of the power grid for reactive power (experiment).

10. Conclusions

The article presents a complete control algorithm for the AC/DC/AC converter connecting the induction generator with the power grid. The algorithm for controlling the DC/AC converter from the power grid does not use measurements of output currents or voltages on the LCL filter capacitors. These values are estimated on the basis of measurements of power grid currents, voltages and filter parameters.

The application of the converter with the proposed control algorithm provided near-sinusoidal currents of the power grid. Thanks to the LCL filter coupling the system with the power grid and the predictive control, the content of higher harmonics in the output current below ~1% was obtained, despite the assumption of high voltage distortion (Figure 19, 20) and limiting the number of measurements of the input quantities. Correct operation of the system was also achieved with the proposed modulator for the multilevel inverter. The system also performs the function of a reactive power compensator thanks to the possibility of controlling the phase of the current in relation to the grid voltage.

However, to control the AC/DC converter from the induction generator side, the algorithm of direct rotor flux and torque control was used. The current distortion on the generator side is slightly higher (Figure 21a) and this is due to the lack of an additional coupling filter (Figure 9). This lack is partially compensated by the relatively high inductance of the induction motor. The low content of higher harmonics of the current does not significantly affect the pulsation of the generator's load torque and increasing losses.

Original simple algorithms of modulators do not require trigonometric functions or arrays for calculations. This reduced the time needed to calculate the switching times of inverter transistors. The use of full processing of the produced energy extends the use of an induction generator to a range of lower wind speeds.

The article proposes a modification of the maximum power point tracking method. It concerns the range of higher wind speeds, in which a change of the angle of the wind turbine blades setting is required. The modification was implemented by introducing the correction factor c_β to the dependence (3). This enabled the use of an induction generator with a maximum power factor C_p for wind speeds varying within wide limits.

In the studies, the presented system was characterised by high efficiency, which for different loads and operating systems is shown in Table 2.

Table 2. Total efficiency of generator systems.

	With all measurements	Without measurement u_c	Without measurement u_c, i_f
P_s [kW]	η %	η %	η %
1.6	91.02	91.02	91.07
5.5	92.74	92.74	92.67
10.0	91.77	91.77	91.75

The promising results of the system test encourage further work. The high complexity of the control algorithm presented in the article requires the use of a microprocessor

controller with high computing power. Therefore, also all the required computational procedures were written in the "C" programming language with a minimum number of instructions. It guarantees on relatively short control times in the real system.

The proposed system was characterized by fewer measurements than are required in typical systems. By using estimation and prediction, the number of measurement channels was reduced by four. At the same time, the system did not show oscillations or a significant increase in the content of higher harmonics in the power grid current. The efficiency of the system also did not noticeably deteriorate. At the same time, the reduced number of measurements increases reliability and reduces implementation costs. The applied control method does not require additional damping resistances in the LCL coupling circuit. At the stage of practical implementation of the control, the requirements for the selection of a microprocessor controller are also fully acceptable.

Author Contributions: Author Contributions: Conceptualization: R.S.; Formal analysis: A.K.; Validation: A.K. and R.S.; Methodology: A.K.; Investigation: A.K.; Writing: A.K. and R.S.; Project administration and Funding acquisition: R.S. All authors have read and agreed to the published version of the manuscript

Conflicts of Interest: "The funders had no role in the design of the study; in the collection, analyses, or interpretation of data; in the writing of the manuscript, or in the decision to publish the results".

Appendix A

Induction motor (Generator):

BBC QV 160M4AA

P_N = 11 kW, U_{1N} = 400 V(l-l), I_{1N} = 22,5 A,
f_{1N} = 50 Hz, n_N = 1438 rpm,   2p = 4, $\cos\varphi_N$ = 0,83

Parameters of motor:

R_s = 0,3223 Ω, $L_{\sigma s}$ = 1,99 mH, R_r = 0,4762 Ω,
$L_{\sigma r}$ = 3,4 mH, L_m = 69,69 mH,   J = 0,194 kgm²

Parameters of *LCL* filter:

R_f = 0,1 Ω, L_f = 2,0 mH, R_s = 0,05 Ω, L_s = 1,0 mH, C_f = 10,0 μF

References

1. Sikorski A., Kuźma A., Cooperation of induction squirrel-cage generator with grid connected AC/DC/AC converter, Bulletin of the Polish Academy of Sciences: Technical Sciences 57 (4), 2009, 317-322.
2. Sikorski A., Korzeniewski M., Malinowski M., AC/DC/AC converter in small hydropower station, Electrotechnical review, ISSN 0033-2097, R. 87 Nr 6/2011, 97-100, (in Polish).
3. Béchir B., Faouzi B., Gasmi M., Wind energy conversion system with full-scale power converter and squirrel cage induction generator, International Journal of Physical Sciences, Vol. 7(46), No 9, 2012, 6093-6104.
4. SimõesM.G., Farret F.A., Renewable Energy Systems: Design and Analysis with Induction Generators, CRC Press, 2004, Power Electronics and Applications Series
5. Rodriguez J., Pont J., Lezana P., Kouro S., Tutorial on Multilevel Converters, International Conference on Power Electronics and Intelligent Control for Energy Conservation, Warsaw, 17-19 October, 2005
6. Kot R., Rolak M., Malinowski M., Comparison of maximum peak Power cracking algorithms for a small wind turbine, Mathematics and Computers in Simulation, No 91, 2013, 29-40.
7. Serhoud H., Benattous D., Maximal Wind Energy Tracing of Brushless Doubly-Fed Generator under Flux Oriented Vector Control, International Journal of Renewable Energy Research, Vol.2, No.2, 2012, 243-249.
8. Koutroulis E., Kalaitzakis K., Design of Maximum Power Tracking System for Wind-Energy-Conversion Applications, IEEE Transactions on Industrial Electronics, Vol. 53, No 2, 2006, 486-494.

9. Aouzellag D., Ghedams K., Berkouk E. M., Power Control of a Variable Speed Wind Turbine Driving an DFIG, Renewable Energies and Power Quality Journal, Vol. 1, No. 4, 2006, 31-35.

10. El-Sousy F. F. M., Orabi M., Godah H., Maximum Power Point Tracking Control Scheme for Grid Connected Variable Speed Wind Driven Self-Excited Induction Generator, Journal of Power Electronics, Vol. 6, No. 1, 2006, 52-66.

11. Agarwal V., Aggarwal R.K., Patidar P., Patki Ch., A Novel Scheme for Rapid Tracking of Maximum Power Point in Wind Energy Generation Systems, IEEE Transactions on Energy Conversion, Vol. 25, No 1, 2010, 228-236.

12. El-Sousy F.F., Orabi M., Godah H., Maximum Power Point Tracking Control Scheme for Grid Connected Variable Speed Wind Driven Self-Excited Induction Generator, Journal of Power Electronics, Vol. 6, No. 1, January 2006

13. Strzelecki R., Szczepankowski P., Parchomiuk M., Grabarek M., Two-way converter 4L-DC with active voltage control in intermediate circuit, Electrotechnical review, ISSN 0033-2097, R. 88 Nr 12a/2012, 12-17, (in Polish).

14. Akagi H., Kanazawa Y., Nabae A., Generalized theory of the instantaneous reactive power in three-phase circuits, Conf. Rec. IEEJ-IPEC, (1983), 1375–1386.

15. Akagi H., Watanabe E.H., Aredes M., Instantaneous Power Theory and Applications to Power Conditioning, Wiley-IEEE Press, Power, Energy and Industry Applications, 2007

16. Wojciechowski D., Control system for parallel active filter with coupling LCL circuit, Electrotechnical review, ISSN 0033-2097, R. 86, Nr 2, 2010, 65-70, (in Polish).

17. Holmes D.G., Martin D.A., Implementation of a Direct Digital Predictive Current Controller for Single and Three Phase Voltage Source Inverter, IAS '96. Conference Record of the 1996 IEEE Industry Applications Conference Thirty-First IAS Annual Meeting, 06-10 October 1996, San Diego, CA, USA

18. Rodriguez J., Cortes P., Predictive Control of Power Converters and Electrical Drives, Wiley-IEEE Press, Power, Energy and Industry Applications, 2012

19. Kouro, S.; Perez, M.A.; Rodriguez, J.; Llor, A.M.; Young, H.A. Model Predictive Control: MPC's Role in the Evolution of Power Electronics. IEEE Ind. Electron. Mag. 2015, 9, 8–21.

20. Falkowski, P.; Sikorski, A. Finite Control Set Model Predictive Control for Grid-Connected AC—DC Converters with LCL Filter. IEEE Trans. Ind. Electron. 2018, 65, 2844–2852.

21. Hu, J.; Shan, Y.; Guerrero, J.M.; Ioinovici, A.; Chan, K.W.; Rodriguez, J. Model predictive control of microgrids–An overview. Renew. Sustain. Energy Rev. 2021, 136, 110422.

22. Wojciechowski D, Strzelecki R., Predictive Control of Active Filter System with LCL Coupling Circuit, The 2010 International Power Electronics Conference, Sapporo, Japan, 21–24 June 2010

23. Kasprowicz A., Voltage and frequency stabilisation system of self-excited induction generator, Electrotechnical review, ISSN 0033-2097, R. 92 Nr 12/2016, 296-301, (in Polish).

24. Souza H., Neves F., Cavalcanti M., Bueno E., Rizo M., Frequency Adaptive Phase-Sequence Separation Method Based on a Generalized Delayed Signal Cancelation Method, 2009 IEEE Energy Conversion Congress and Exposition

25. Wang Y.F., Li Y. W., Grid Synchronization PLL Based on Cascaded Delayed Signal Cancellation, IEEE Transactions on Power Electronics, Vol. 26, No. 7, July 2011

26. Wang Y.F., Li Y. W., Analysis and Digital Implementation of Cascaded Delayed-Signal-Cancelation PLL, IEEE Transactions on Power Electronics, Vol. 26, No 4, 2011, 1067-1080.

27. Bobrowska-Rafał M., Rafał K., Jasiński M., Kaźmierkowski M.P., Grid synchronization and symmetrical components extraction with PLL algorithm for grid connected power electronic converters – a review, Bulletin of the Polish Academy of Sciences: Technical Sciences, Vol. 59, No. 4, 2011, 485-497.

28. Wang Y.F., Li Y. W, Three-Phase Cascaded Delayed Signal Cancellation PLL for Fast Selective Harmonic Detection, IEEE Transactions on Industrial Electronics, Vol. 60, No 4, 2013, 1452-1463.